APL Materials

RESEARCH ARTICLE | JUNE 15 2023

Accurate determination of band tail properties in amorphous semiconductor thin film with Kelvin probe force microscopy

Luca Fabbri ; Camilla Bordoni ; Pedro Barquinha ; Jerome Crocco; Beatrice Fraboni ;
Tobias Cramer

APL Mater. 11, 061123 (2023)
https://doi.org/10.1063/5.0151367

19 April 2024 01:59:51

APL Materials ARTICLE scitation.org/journal/apm

Accurate determination of band tail properties in amorphous semiconductor thin film with Kelvin probe force microscopy

Cite as: APL Mater. 11, 061123 (2023); doi: 10.1063/5.0151367
Submitted: 21 March 2023 • Accepted: 5 June 2023 •
Published Online: 15 June 2023

Luca Fabbri,[1] Camilla Bordoni,[1] Pedro Barquinha,[2] Jerome Crocco,[3] Beatrice Fraboni,[1] and Tobias Cramer[1,a)]

AFFILIATIONS

[1] Department of Physics and Astronomy, University of Bologna, Viale Berti Pichat 6/2, 40127 Bologna, Italy
[2] CENIMAT|i3N and CEMOP/UNINOVA, NOVA School of Science and Technology, Campus de Caparica, NOVA University Lisbon, 2829-516 Caparica, Portugal
[3] DPIX, 1635 Aeroplaza Dr., Colorado Springs, Colorado 80916, USA

[a)] Author to whom correspondence should be addressed: tobias.cramer@unibo.it

ABSTRACT

The disordered microscopic structure of amorphous semiconductors causes the formation of band tails in the density of states (DOS) that strongly affect charge transport properties. Such band tail properties are crucial for understanding and optimizing thin-film device performance with immense relevance for large area electronics. Among the available techniques to measure the DOS, Kelvin Probe Force Microscopy (KPFM) is exceptional as it enables precise local electronic investigations combined with microscopic imaging. However, a model to interpret KPFM spectroscopy data on amorphous semiconductors of finite thickness is lacking. To address this issue, we provide an analytical solution to the Poisson equation for a metal–insulator–semiconductor junction interacting with the atomic force microscope tip. The solution enables us to fit experimental data for semiconductors with finite thickness and to obtain DOS parameters, such as band tail width, doping density, and flat band potential. To demonstrate our method, we perform KPFM experiments on Indium–Gallium–Zinc Oxide (IGZO) thin-film transistors (IGZO-TFTs). DOS parameters compare well with values obtained with photocurrent spectroscopy. We demonstrate the relevance of the developed method by investigating the impact of ionizing radiation on DOS parameters and TFT performance. Our results provide clear evidence that the observed shift in threshold voltage is caused by static charge in the gate dielectric, leading to a shift in flat band potential. Band-tails and doping density are not affected by the radiation. The developed methodology can be easily translated to different semiconductor materials and paves the way for quantitative microscopic mapping of local DOS parameters in thin-film devices.

© 2023 Author(s). All article content, except where otherwise noted, is licensed under a Creative Commons Attribution (CC BY) license (http://creativecommons.org/licenses/by/4.0/). https://doi.org/10.1063/5.0151367

19 April 2024 01:59:51

INTRODUCTION

Amorphous semiconductors are fundamental for large area electronic devices, such as active matrices in detectors or displays. The disordered structure of the amorphous phase causes the formation of localized states at the edges of the valence and conduction bands, called band tails. Such band tails are of fundamental importance for the transport properties of the material since they act as trapping states for carriers.[1] An important technological aim is the downscaling of amorphous semiconductor device dimensions, where local border effects become increasingly relevant. In such a situation, band-tails and general density of states (DOS) properties have to be understood as local properties that are influenced by local variations in the microstructure, chemical composition, or electrostatic charge trapping. However, most techniques that assess DOS properties rely on macroscopic probes and quantify average material properties. Examples are spectroscopic methods that measure absorption or photocurrent generation as well as electrical methods based on capacitance or transistor measurements and modeling.[2–7] Instead, a microscopic technique that could reveal

© Author(s) 2023

DOS properties with nanometric resolution on working microstructured semiconductor thin-film devices is highly wanted to improve device understanding and optimization.

Kelvin Probe Force Microscopy (KPFM) is an advanced atomic force microscopy technique that can measure electrical properties of a sample with high resolution and precision, including the density of states.[8–11] With KPFM, one measures the contact potential difference between the tip and the sample.[12] This quantity is related to the amount of charge injected into the surface layer.[13] However, the relationship is complex because of band bending and non-uniform charge distribution.[14] Despite these issues, KPFM has been successfully applied to study different phenomena in amorphous semiconductors.[15–17] Examples are the measurement of the surface potential in thin-film transistors (TFTs)[18,19] or the determination of the DOS in ultrathin semiconducting layers where band bending is not relevant.[20,21] For instance, Roelofs *et al.* demonstrated quantitative measurements in a molecular semiconducting layer built by self-assembly without any prior assumption on the density of states.[20] Zhang *et al.* demonstrated the formation of trap states at the SiO_2–oligothiophene monolayer interface and obtained the doping density and sign of charge carriers using KPFM.[21] For semiconducting layers of finite thickness, the interpretation of KPFM measurements requires the solution of the non-linear Poisson equation to describe band bending correctly.[22] So far, a possible numerical solution was only described by Germs *et al.* in their study on amorphous oxide semiconductors, where they proposed an iterative procedure to approximate the DOS for these materials.[23] Despite this progress, a reliable analytical model to derive the DOS from KPFM measurements in amorphous semiconductors with a finite layer thickness is not available.

One of the most promising amorphous semiconductors is Indium–Gallium–Zinc Oxide (IGZO), as it can be easily deposited by sputtering and presents a mobility of the order of 10 cm^2/Vs, which is ten times higher than amorphous silicon.[24] IGZO has a reduced band tail width with respect to a-Si, and this finding is related to the increased mobility.[25] Band tails in IGZO can be modeled as exponentials described by two parameters: the band tail width and the oxygen vacancy doping density. This assumption is confirmed by experimental studies.[1,2,26] In addition to its high mobility, IGZO is characterized by a larger bandgap than a-Si, causing a low off-state current and a high transparency. These properties make IGZO it an ideal material for use in transparent electronics such as flexible displays and sensors.[24] Investigations of the DOS properties of IGZO have been performed by several groups, employing a wide range of techniques.[2,3,26]

The aim of this study is to achieve reliable local measurements of the amorphous band tail in IGZO using Kelvin Probe Force Microscopy (KPFM). We analyze KPFM spectroscopy data with a model based on the solution of the non-linear Poisson equation for the metal–insulator–semiconductor (MIS) junction. The model is analytical and allows for a direct fit of the experimental data, providing values for the relevant DOS parameters, such as the band tail width E_t, the doping density N_D, and the flat band potential V_{FB}. We validate the accuracy of our method by comparing it to photocurrent spectroscopy measurements. We further demonstrate the value of our method by analyzing the effect of ionizing radiation on DOS properties.

RESULTS

The standard configuration for KPFM experiments on thin-film semiconductor devices is depicted in Fig. 1(a). The KPFM tip is operated above the exposed semiconducting thin film. The source and drain electrodes contact the semiconducting layer, and a field effect is exerted by the gate electrode, separated from the semiconductor by a thin dielectric layer. The source is connected to the ground, while potentials V_D and V_G applied to the drain and the gate are controlled by a source measurement unit. The KPFM experiment probes the local surface morphology of the semiconducting channel and measures the local surface voltage, V_{KPFM}. Depending on the applied gate voltage, two limiting cases of the surface voltage have to be considered: In depletion, the channel is void of carriers and behaves as a dielectric; the electric field of the gate penetrates without screening the semiconductor and interacts with the KPFM tip. The surface voltage varies with the applied gate voltage. In contrast, in accumulation, the semiconducting layer behaves as a conductor, and its carriers screen the gate field. Accordingly, surface voltage is constant. KPFM spectroscopy experiments that aim at probing the DOS of the semiconductor, characterize the surface voltage as a function of the gate voltage while the transition from depletion to accumulation occurs.

In order to derive a quantitative model for KPFM spectroscopy on the semiconducting thin film, we consider the schematic energy diagram of the MIS junction during the interaction with the Atomic Force Microscope (AFM) tip as shown in Fig. 1(b). All relevant energetic parameters are indicated in the diagram. We distinguish two cases: first, the flat band condition that is drawn in gray lines. Second, the depletion condition is highlighted with black lines. The solid lines refer to energy levels, while the dashed lines stand for vacuum levels. The Fermi level in the semiconductor is given by the grounded source electrode and is colored red in the diagram. The application of a voltage to the gate produces band bending inside the semiconductor. This effect is quantified with the potential $\phi(x)$, which expresses the shift of vacuum level in the semiconductor with respect to the flat band condition. The spatial coordinate of $\phi(x)$ starts at the external interface $\phi(x = 0) = \phi_0$ and ends at the interface with the gate dielectric $\phi(x = t) = \phi_t$. Here, t denotes the thickness of the semiconducting layer. Other important parameters in the diagram regard the drop in vacuum level across the gate dielectric V_{ox} and the work functions of the gate and source electrodes, Φ_g and Φ_s, respectively. Additional offsets in vacuum level occur at interfaces due to static trapped charges or interfacial dipoles. They are denoted as ϕ_{ds} and ϕ_{dg} and refer to the interfaces source/semiconductor and gate/dielectric, respectively. Finally, the diagram includes the AFM probe interacting electrostatically with the MIS junction. The potential V_{KPFM} is controlled by the KPFM feedback loop targeting the absence of electrostatic forces between the tip and the sample. Accordingly, there is no electric field between the tip and the semiconductor surface, and the vacuum level of the AFM tip aligns with the semiconductor interface. The measured V_{KPFM} thus reports on changes in vacuum level at the external semiconductor interface occurring when the gate voltage is changed.[14] Based on the energy diagram, we derive the quantitative model for the KPFM experiment in two steps. First, we develop the relation for the potential $\phi(x)$ describing band bending in an amorphous

19 April 2024 01:59:51

© Author(s) 2023

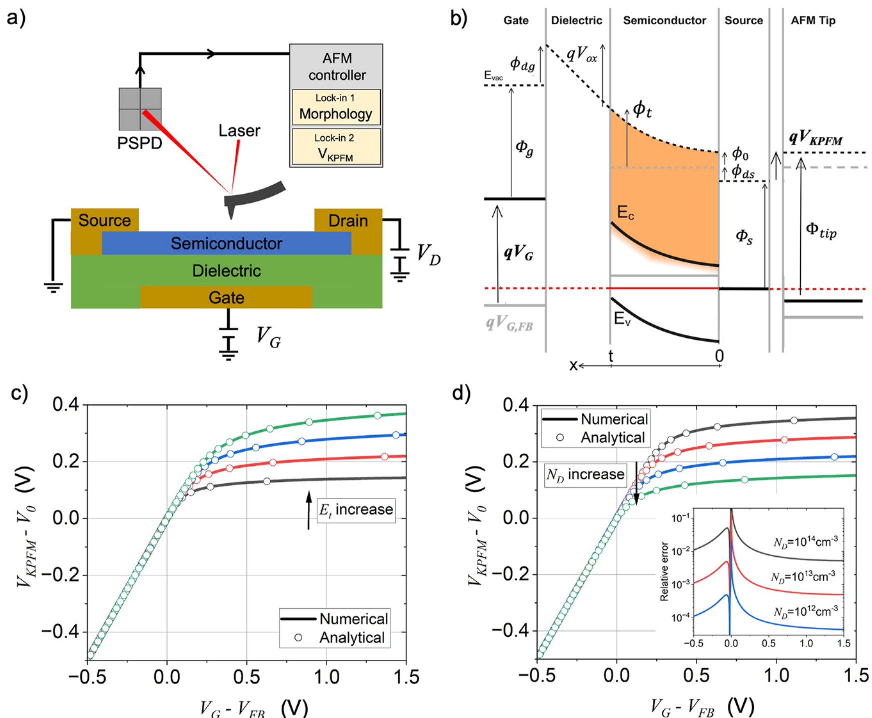

FIG. 1. KPFM spectroscopy and model: (a) Schematic of the Kelvin Probe Force Microscopy experiment performed on working thin-film transistors. In the KPFM spectroscopy experiments, the tip potential is measured while the transistor gate voltage is varied. (b) Schematic band diagram of the metal–insulator–semiconductor junction interacting with the AFM tip. The gray color corresponds to the flat band condition. The energy levels in depletion are depicted in black. The semiconductor is grounded through the source. The AFM tip is interacting with the semiconductor. (c) and (d) Simulated KPFM spectroscopy measurements. The solutions to Poisson's equation are shown for different values of band tail width E_t ranging from 20 to 50 meV with fixed doping densities $N_D = 10^{12}$ cm^{-3} in (c) and different values of N_D ranging from 10^{11}–10^{14} cm^{-3} and fixed E_t = 30 meV in (d). The inset shows the calculated error between the numerical and analytical solutions for different trap densities.

19 April 2024 01:59:51

semiconductor of finite thickness. Second, we identify how the experimental observables V_{KPFM} and V_G are linked to the parameters entering the potential function $\phi(x)$. We note that we do not distinguish for KPFM experiments between trap states or conducting states, as both contribute to local charge accumulation and, hence, contribute to changes in KPFM surface potential. Accordingly, the model also fully includes Fermi-level pinning effects occurring at semiconductor interfaces.

Band bending occurs due to the buildup of local space charge $\rho(x)$ in the semiconductor. For an n-doped amorphous semiconductor, we can write

$$\rho(x) = q_0 N_D\left[1 - \exp\left(\frac{\phi(x)}{E_t}\right)\right], \tag{1}$$

where E_t describes the exponential band tail,[25,27] $DOS(E) \propto \exp(E/E_t)$, N_D introduces the concentration of n-type doping sites, and q_0 refers to the unit charge. Equation (1) is derived from the solution of the Fermi–Dirac integral under the zero-temperature assumption. The finite temperatures can be accounted for as a temperature dependent shift in the flat band voltage. The equation for $\phi(x)$ is then defined by combining (1) with the Poisson equation,

$$\frac{d^2\phi(x)}{dx^2} = -\frac{\rho(x)}{\varepsilon\varepsilon_0}. \tag{2}$$

The resulting differential equation requires two boundary conditions to provide a unique solution for $\phi(x)$. Following our KPFM experiment, we consider the external semiconductor interface at $x = 0$, where we nullify the electric field and measure the local surface potential. Accordingly, we set $\phi(x = 0) = \phi_0$ and $\phi'(x = 0) = 0$. For these boundary conditions, we obtain an analytical solution for the condition $\phi(x = 0) \gg E_t$,

$$\phi(x) = E_t \log\left\{\exp\left(\frac{\phi_0}{E_t}\right)\left(\tan^2\left[\frac{x}{\lambda\sqrt{2}}\exp\left(\frac{\phi_0}{2E_t}\right)\right] + 1\right)\right\}. \tag{3}$$

Here, $\lambda = \sqrt{E_t\varepsilon\varepsilon_0/q_0^2 N_D}$ describes a characteristic length scale of the semiconductor. The solution describes the band bending occurring when negative carriers accumulate in the channel and strongly screen the gate field, and it depends explicitly on the DOS parameters. Below, we compare the analytical solution with the complete numerical one and show that it is, in many situations, also a good

© Author(s) 2023

approximation to describe KPFM experiments in the depletion regime.

In the second part of our derivation, we link the potential function $\phi(x)$ to the experimental observables V_G and V_{KPFM}. Key to this are the function values at the external and internal semiconductor interfaces: $\phi(x=0)=\phi_0$ and $\phi(x=t)=\phi_t$, respectively. When a potential is applied to the gate, the vacuum level and the conduction band edge are shifted, and due to the finite thickness of the semiconductor, a residual of the gate electric field can reach the external semiconductor interface. The resulting shift in the conduction band is ϕ_0, and it is directly related to the voltage V_{KPFM} measured at the AFM tip in the KPFM experiment. A direct measurement of ϕ_0 is difficult as different offsets contribute to V_{KPFM}, such as the work function of the AFM-tip, the possible dipole layer forming at the semiconductor interface, and amplifier offsets in the KPFM signal acquisition. Accordingly, we introduce the Kelvin probe surface voltage measured in flat band conditions, $V_{KPFM,FB}$, and obtain

$$\phi_0 = V_{KPFM} - V_{KPFM,FB}. \tag{4}$$

Next, we consider the semiconductor interface with the gate dielectric and derive the relation that links the surface voltage ϕ_t to the gate voltage V_G. Following the energy diagram in Fig. 1(b), we find

$$qV_G = qV_{G,FB} + \phi_t + qV_{ox}. \tag{5}$$

Here, V_G is the flat band voltage and V_{ox} is the potential drop over the gate dielectric, which is given by $V_{ox}=\sigma/c_{ox}$. The capacitance of the gate dielectric c_{ox} is a constant, and the surface charge density in the semiconducting channel σ can be directly computed from the potential function $\phi(x)$ (see the supplementary material). We note that Eq. (3) allows us to express both ϕ_t and σ as a function of ϕ_0. Accordingly, the combination of Eqs. (3)–(5) provides an analytical expression for V_G as a function of V_{KPFM}.

Figures 1(c) and 1(d) show the simulated V_{KPFM} vs V_G curves for different combinations of DOS parameters. At negative gate voltages, when the channel is in depletion, a linear relation with a unitary slope is observed as the gate field passes through the semiconductor. Instead, toward positive gate voltages, the curve flattens and reaches a plateau. V_{KPFM} becomes independent of V_G as the gate field is fully screened in the semiconducting channel. Figure 1(c) demonstrates how the parameter E_t, describing the width of the conduction band tail, strongly impacts the shape of the curves. Wider band tails (larger E_t) cause a wider transition from full depletion to full accumulation and, hence, a reduced curvature of the V_{KPFM} vs V_G curve. Accordingly, the plateau is reached at higher KPFM voltages. In contrast, the parameter describing the dopant concentration N_D has a different effect, as shown in Fig. 1(d). The shape of the V_{KPFM} vs V_G curve is not altered with N_D, but higher values cause a shift of the curve to lower values of V_{KPFM}. Due to the high dopant concentration, more charge carriers are in the channel at flat band potential and full screening of the gate field occurs already at smaller shifts in the vacuum level. The two graphs also show excellent agreement between the numerical and approximated analytical solutions for the tested combinations of DOS parameters. Interestingly, for a wide range of DOS parameters, the analytical solution turns out to be also a good approximation in depletion condition even though the condition $\phi \gg E_t$ is no longer valid. The relative error of the approximate analytical solution is largest in flat band condition and increases at higher doping concentrations N_D.

The simulations show that the band tail width E_t can be determined from experimental data as it directly impacts the shape of the V_{KPFM} vs V_G curves. In contrast, the doping density N_D is not uniquely determined by the curve. Changes in N_D only translate the curve, and variations in the flat band offset parameters $V_{G,FB}$ and $V_{KPFM,FB}$ have the same effect. In order to determine N_D, additional data need to be considered, and here, we describe two possible approaches: First, flat band voltage $V_{G,FB}$ can also be measured with alternative techniques, such as capacitance measurements. Subsequently, also $V_{KPFM,FB}$ and N_D can be obtained from the data. However, capacitance measurements are not always feasible, and border effects in small transistor channels can make their interpretation difficult. Therefore, we follow a second approach that aims at determining $V_{KPFM,FB}$ with additional KPFM measurements done on the source electrode. Following the energy diagram in Fig. 1(b), one can write $V_{KPFM,FB} = V_{KPFM,s} + \phi_{ds}$. Here, ϕ_{ds} is the barrier that charge carriers have to overcome when injection or extraction occurs from the semiconducting channel. As transport in optimized TFTs is not limited by contact effects, as shown experimentally, we can assume that $\phi_{ds} < k_B T$ and exploit this assumption in the determination of $V_{KPFM,FB}$ and, subsequently, N_D. The measurement of $V_{KPFM,s}$ is easily achieved in the same experiment, as it is enough to enlarge the scanning area to include part of the source electrodes.

To test our model, we perform KPFM experiments on indium–gallium–zinc oxide (IGZO) thin film transistors with a 60 nm thick semiconducting layer and a dielectric composed of 80 nm of Ta_2O_5 and 20 nm of Al_2O_3. The source and drain contacts are made of molybdenum, as is the gate electrode. The channel has a geometry of $W = 320$ μm and $L = 20$ μm. The optical microscope image of the device is reported in Fig. 2(a). In this device, the gate is placed below the channel while the source and drain electrodes are deposited on top, as reported in Fig. 2(a). Figure 2(b) shows the transfer characteristics of the device. We measured a mobility of (7.3 ± 0.2) cm^2/V s and a subthreshold slope of $(0.12 \pm 0.02)V/$decade. Microscopic images of the channel as obtained by KPFM in amplitude modulation mode are shown in Figs. 2(c) and 2(e). In the height map, one clearly recognizes the channel and the source and drain electrodes. The V_{KPFM} map was obtained with $V_G = -2.7$ V and $V_D = 0.1$ V. Accordingly, the channel shows a negative potential, confirming the penetration of the gate field and the absence of charge carriers. In Fig. 2(d), we report both the V_{KPFM} and the height profile along the red line in Figs. 2(c) and 2(e). For comparison, the KPFM base line obtained at $V_G = 0$ V is also shown in the profile. The KPFM data show that close to the contacts, electrostatic interactions with the source electrodes limit the measurements, but inside the channel, a flat and constant potential is measured.

Next, we continue with KPFM spectroscopic measurements done at a single position in the center of the channel to determine the IGZO's DOS parameters. Figure 3(a) shows the measurement of V_{KPFM} obtained in the channel while the gate voltage V_G was swept from −1 to 5 V. On the source electrode, we obtain a constant value of $V_{KPFM,s}$=0.02 V, and the value is indicated in the plot to mark the flat band potential condition at $V_{G,FB} = (2.8 \pm 0.2)V$. With this condition, the model fits well and uniquely to the experimental data,

19 April 2024 01:59:51

© Author(s) 2023

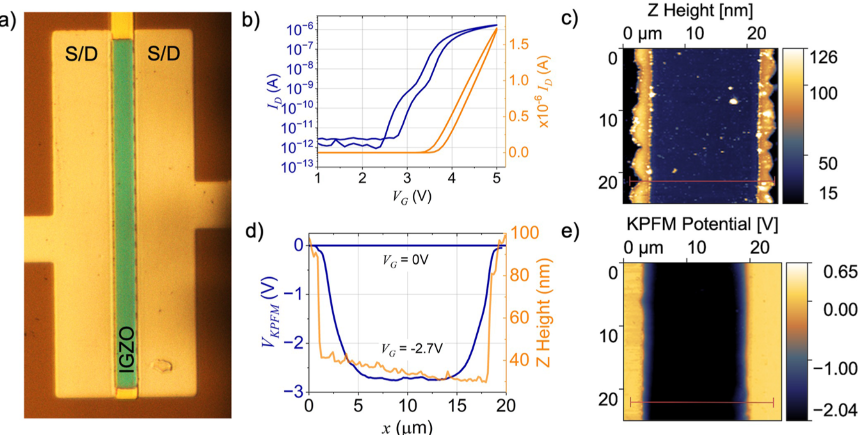

FIG. 2. (a) Optical microscope image of an a-IGZO thin film transistor with channel geometry of $320 \times 20\ \mu m^2$. The source and drain electrodes are deposited on the top of the device, while the gate is under the semiconducting channel. (b) Transfer characteristics in log scale (blue) and linear scale (orange). (c) AFM height map of the channel. (d) KPFM potential and morphology profiles of the sample. The profile line is identified with the red marker in subfigures (c) and (e). (e) KPFM potential map of the channel at $V_G = -2.7$ V.

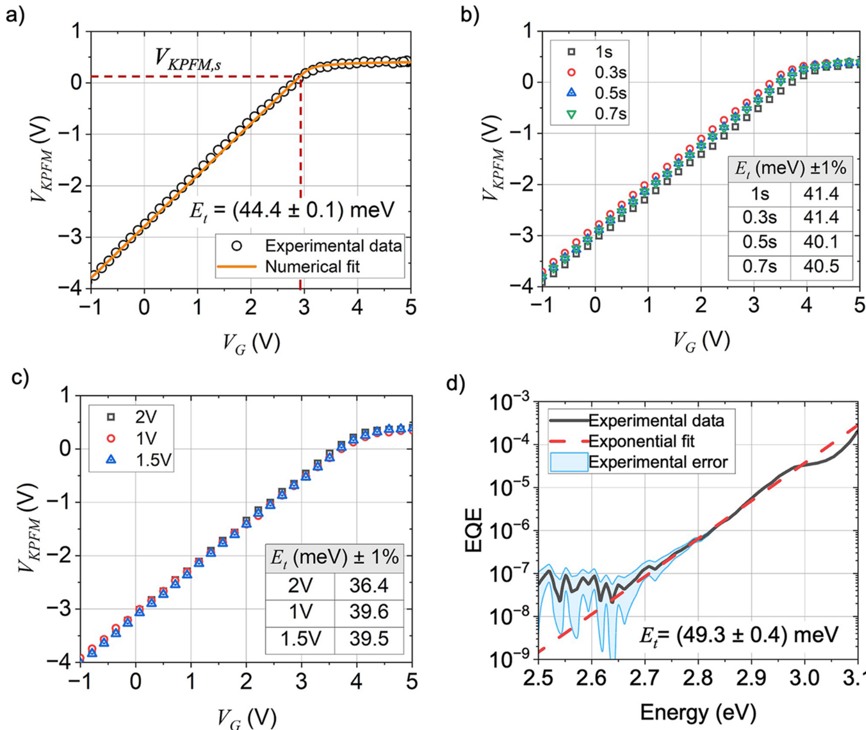

FIG. 3. KPFM spectroscopy and fit to the model: (a) Example of an experimental V_{KPFM} vs V_G curve and fit to the model with an extracted value of band tail width, E_t. The red dashed line shows the KPFM potential measured on the source electrode and allows us to extract the flat band potential. (b) Plot of the KPFM curve for different values of sweep time and fixed AC driving voltage with fitted values of band tail width (inset). (c) Plot of the KPFM curve for different values of AC driving voltage and a fixed sweep time of 1 s. The fitted values of E_t are reported in the inset table. (d) Plot of the photocurrent external quantum efficiency (EQE) spectrum measured on the IGZO thin film transistor. The band tail width is obtained by the linear fit in the interval 2.7–3.0 eV. At lower photon energies, the noise background dominates the signal.

19 April 2024 01:59:51

© Author(s) 2023

TABLE I. Comparison of DOS parameters extracted from both this work and the literature with different experimental techniques.[30,31]

Experiment	Type	N_D (cm^{-3})	E_t (meV)
This work	KPFM	$(1.1 \pm 0.6) \times 10^{12}$	44.4 ± 0.1
Tsuji *et al.*	CV	1.2×10^{17}	80
Jeon *et al.*	Simulated	5×10^{16}	67
This work	Photocurrent	⋯	49.3 ± 0.4

yielding a band tail width $E_t = (44.4 \pm 0.1)$ meV and a doping density of $N_D = (1.4 \pm 0.6) \times 10^{12}$ cm^{-3}. The values are stable, and variations of experimental parameters, such as KPFM tip bias amplitude V_{AC} or sweep time, do not have a significant impact on the obtained values, as shown in Figs. 3(b) and 3(c). In this regard, the stability toward variations in V_{AC} also confirms that the contact potential difference (CPD) interpretation of KPFM measurements in semiconductors is correct and the linear response is maintained.[14]

The extracted DOS parameters can be compared to values obtained with different, not microscopic, techniques, as done in Table I. Our estimates of band tail width E_t and doping density N_D are lower than values found in the literature with capacitance measurements. We note that differences in the fabrication protocol of the IGZO film might explain such variations.[28] In particular, the amount of oxygen vacancy density strongly depends on the conditions during semiconductor deposition and annealing. For instance, a reduced number of oxygen vacancies are expected in a more crystalline IGZO sample.[29] To provide an alternative characterization of the conduction band tail in the tested transistor structures, we conduct photocurrent spectroscopy experiments. Figure 3(d) reports the external quantum efficiency (EQE) in photocurrent measured at different photonic excitation energies. A linear dependence is observed on the logarithmic plot and fits an exponential with a characteristic energy of $E_t(PC) = (49.3 \pm 0.4)$ meV. This finding is in excellent agreement with the KPFM value. A slightly higher value from photocurrent spectroscopy is expected due to the contribution of the valence band tail.

Finally, we demonstrate the relevance of our technique for understanding TFT stability and degradation. An example is the x-ray induced radiation damage causing a shift to negative voltages.[32] Such an effect is critical for different radiation related applications, such as the degradation of active-matrix detector backplanes or the sensitivity of microelectronic dosimeters. Despite this relevance, two basic mechanisms can potentially explain the negative shift. On the one hand, one can assume that ionizing radiation impinges on the semiconductor and causes the generation of oxygen vacancies acting as additional doping sites. Consequently, more carriers are in the channel at flat band potential, and a more negative gate voltage is needed to switch-off the channel. On the other hand, ionizing radiation is known to cause positive space-charge build-up in wide band-gap oxide dielectrics. The reason is that the x-ray generated hole and electron carriers behave differently in these dielectrics. Electrons are mobile and ultimately exit from the dielectric into conductive contact. Hole charges, instead, are trapped and continue to accumulate with increasing exposure doses. The generated positive space charge causes a potential offset in the gate dielectric and shifts the flat band potential to negative values.

To decipher which of the two possible causes is relevant, we perform KPFM experiments on TFTs before and after exposure to a total dose of 400 mGy. The transfer characteristics of the device, reported in Fig. 4(a), in the pristine and irradiated conditions show a clear shift in threshold of $\Delta V_{th} = (-1.10 \pm 0.01)V$. The corresponding KPFM spectroscopy measurements are shown in Fig. 4(b) together with the fits to our model. The extracted parameters are reported in Table II. We note that both N_D and E_t are not modified during the exposition, while the flat band potential V_{FB} is reduced. The shift is $\Delta V_{FB} = (-1.0 \pm 0.2)V$, which is coherent with the measured shift in the threshold voltage. We can conclude that the DOS parameters are not modified by x-ray irradiation; therefore, the effect of x-rays in our device is to generate positive charges in the gate dielectric.

19 April 2024 01:59:51

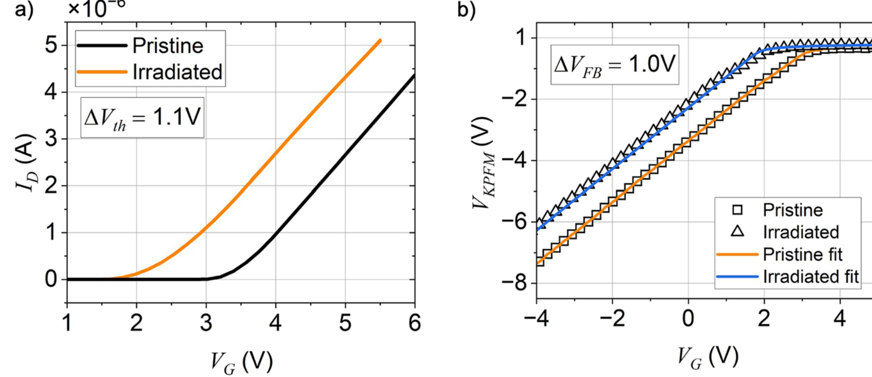

FIG. 4. Investigation of x-ray radiation damage in IGZO TFT. (a) Transfer characteristics before and after exposure to x-ray radiation (400 mGy at energy corresponding to the Mo–K$_\alpha$ peak, E = 17.5 keV). (b) KPFM spectroscopy performed in the center of the channel before and after radiation exposure. The solid lines show the fit to the developed KPFM model.

© Author(s) 2023

TABLE II. Comparison of density of state parameters before and after x-ray irradiation.

Parameter	Pristine	Irradiated
N_D ($\times 10^{12}$ cm^{-3})	1.4 ± 0.6	1.5 ± 0.6
E_t (meV)	44.4 ± 0.1	45.8 ± 0.2
V_{FB} (V)	2.8 ± 0.1	1.8 ± 0.1

CONCLUSIONS

Our work introduces a novel and precise method to determine amorphous semiconductor band tail properties with KPFM spectroscopy. Different from the former approaches, our technique does not assume a constant charge density in the semiconductor as valid only in 2D or molecular thin layers. Instead, we provide an analytical solution of the non-linear Poisson equation for a metal–insulator–semiconductor (MIS) junction interacting with the AFM tip. This solution takes band bending and possible Fermi-level pinning fully into account. The analytical solution enables the direct fit of KPFM spectroscopy data for semiconducting films with finite thickness and the determination of DOS parameters, including band tail width (E_t) and doping density (N_D), as well as the flat band potential. With this method, we analyze IGZO thin film transistors and obtain a local band tail width of $E_t = (44.4 \pm 0.1)$ meV. To verify this result, we conducted photocurrent spectroscopy and found that the results are in excellent agreement. We showcase the utility of our method by investigating the origin of radiation induced threshold voltage shifts in IGZO-TFTs. The KPFM spectroscopy results provide clear evidence that ionizing radiation does not directly impact the semiconducting layer but causes static charge accumulation in the gate dielectric. The developed methodology paves the way for microscopic imaging of DOS parameters in amorphous semiconductor thin films and provides a crucial tool to understand degradation and device physics in semiconductor thin film devices. The analytical solution allows rapid data analysis and does not require elaborate numerical procedures, as needed in imaging experiments. The method can be combined with high resolution KPFM methods, such as sideband or heterodyne techniques, in order to assess the DOS also at device boundaries, which are expected to be crucial for non-ideality effects.

MATERIALS AND METHODS

We fabricated a TFT with a bottom-gate and top-contact structure, using a Corning Eagle glass substrate and patterning the desired structure by photolithography. We deposited a multilayer, multi-component dielectric consisting of 80 nm of Ta_2O_5 and 20 nm of Al_2O_3 using thermal atomic layer deposition (ALD). The 60 nm IGZO layer was sputtered with a composition ratio of 2.5:1.2:1 for In:Ga:Zn onto the dielectric layer. To activate the IGZO layer, we annealed the sample in air at 180 °C. All the electrodes are made of a 60 nm molybdenum layer deposited by magnetron sputtering. All layers were patterned using 365 nm UV photolithography and etched through reactive ion etching (gate electrode and dielectric) and lift-off (semiconductor and source–drain electrodes), resulting in devices with a width-to-length ratio (W/L) of 320 μm/20 μm, as shown in Fig. 2(a). We conducted Kelvin Probe Force Microscopy (KPFM) measurements using the Park NX-10 Atomic Force Microscope (AFM). For this experiment, we employed an NSC36 cantilever made of n-type silicon and coated with a layer of chromium and gold. The cantilever has a typical force constant of 2 N/m and resonates at a frequency of ~130 kHz. We acquired the transfer characteristics with a Keysight B2912A measurement unit. We kept 0.1 V on the drain during every measure to maintain the linear regime, and thus, we obtained transistor parameters by fitting the transfer characteristics to the standard metal oxide semiconductor FET model for the corresponding regime. X-ray radiation was generated by a molybdenum tube, which we operated at a voltage of 60 kVp and a filament current of 395 μA. The sample was positioned at 20 cm from the shutter to achieve a doserate of 60 μGy/s, delivering a total dose of 400 mGy. Photocurrent spectroscopy of IGZOTFTs was done with a xenon lamp coupled to a monochromator to select a single wavelength at a time. We achieved a noise level on the order of nA for photocurrent measurements on the transistor with our apparatus. This led us to observe that the external quantum efficiency becomes unreliable when energies are below 2.7 eV. To prevent any modification of the semiconductor's density of states, we also used a 400 nm UV-filter, effectively eliminating energies higher than ~3 eV. The TFT was biased at $V_D = 0.1$ V and $V_G = 0.1$ V. The resulting photocurrent was amplified using a Femto current amplifier (DLPCA-200) and measured with a lock-in amplifier.

SUPPLEMENTARY MATERIAL

See the supplementary material for additional information.

ACKNOWLEDGMENTS

L.F. and T.C. acknowledge the funding by the EU - NextGenerationEU with funds made available by the National Recovery and Resilience Plan (NRRP) Mission 4, Component 1, Investment 4.1 (MD 351/2022)—NRRP Research. P.B. received funding from FEDER funds through the COMPETE 2020 program and National Funds through FCT—Portuguese Foundation for Science and Technology—under the scope of Project Nos. LA/P/0037/2020, UIDP/50025/2020, and UIDB/50025/2020 and from the European Community's Horizon Europe program under Grant Agreement Nos. 716510 (ERC-2016-StG TREND) and 101082283 (ERC-2022-POC2 FLETRAD).

AUTHOR DECLARATIONS

Conflict of Interest

The authors have no conflicts to disclose.

Author Contributions

Luca Fabbri: Data curation (lead); Investigation (equal); Software (equal); Writing – original draft (lead); Writing – review & editing (equal). **Camilla Bordoni**: Data curation (equal); Investigation

19 April 2024 01:59:51

© Author(s) 2023

(equal); Writing – review & editing (equal). **Pedro Barquinha**: Conceptualization (equal); Funding acquisition (equal); Project administration (equal); Resources (equal); Supervision (equal); Writing – review & editing (equal). **Jerome Crocco**: Conceptualization (equal); Project administration (equal); Resources (equal); Writing – review & editing (equal). **Beatrice Fraboni**: Conceptualization (equal); Funding acquisition (equal); Project administration (equal); Resources (lead); Supervision (equal); Writing – review & editing (equal). **Tobias Cramer**: Conceptualization (lead); Formal analysis (equal); Funding acquisition (equal); Methodology (lead); Project administration (lead); Supervision (lead); Writing – review & editing (lead).

DATA AVAILABILITY

The data that support the findings of this study are available within the article and its supplementary material.

REFERENCES

[1] S. C. Kim, Y. S. Kim, and J. Kanicki, "Density of states of short channel amorphous In–Ga–Zn–O thin-film transistor arrays fabricated using manufacturable processes," Jpn. J. Appl. Phys. **54**(5), 051101 (2015).

[2] C. Chen, K. Abe, H. Kumomi, and J. Kanicki, "Density of states of a-InGaZnO from temperature-dependent field-effect studies," IEEE Trans. Electron Devices **56**(6), 1177–1183 (2009).

[3] H. Bae, S. Jun, C. H. Jo, H. Choi, J. Lee, Y. H. Kim, S. Hwang, H. K. Jeong, I. Hur, W. Kim, D. Yun, E. Hong, H. Seo, D. H. Kim, and D. M. Kim, "Modified conductance method for extraction of subgap density of states in a-IGZO thin-film transistors," IEEE Electron Device Lett. **33**(8), 1138–1140 (2012).

[4] S. Lee, S. Park, S. Kim, Y. Jeon, K. Jeon, J.-H. Park, J. Park, I. Song, C. J. Kim, Y. Park, D. M. Kim, and D. H. Kim, "Extraction of subgap density of states in amorphous InGaZnO thin-film transistors by using multifrequency capacitance–voltage characteristics," IEEE Electron Device Lett. **31**(3), 231–233 (2010).

[5] W. Wang, P. Wang, and M. Dai, "Simplification of sub-gap density of states extraction method for amorphous In-Ga-Zn-O thin-film transistors by a single capacitance-voltage curve," Microelectron. Reliab. **83**, 111–114 (2018).

[6] K. Jeon, C. Kim, I. Song, J. Park, S. Kim, S. Kim, Y. Park, J.-H. Park, S. Lee, D. M. Kim, and D. H. Kim, "Modeling of amorphous InGaZnO thin-film transistors based on the density of states extracted from the optical response of capacitance-voltage characteristics," Appl. Phys. Lett. **93**(18), 182102 (2008).

[7] J.-H. Park, K. Jeon, S. Lee, S. Kim, S. Kim, I. Song, C. J. Kim, J. Park, Y. Park, D. M. Kim, and D. H. Kim, "Extraction of density of states in amorphous GaInZnO thin-film transistors by combining an optical charge pumping and capacitance–voltage characteristics," IEEE Electron Device Lett. **29**(12), 1292–1295 (2008).

[8] T. Cramer, L. Travaglini, S. Lai, L. Patruno, S. de Miranda, A. Bonfiglio, P. Cosseddu, and B. Fraboni, "Direct imaging of defect formation in strained organic flexible electronics by Scanning Kelvin Probe Microscopy," Sci. Rep. **6**(1), 38203 (2016).

[9] O. Tal, Y. Rosenwaks, Y. Preezant, N. Tessler, C. K. Chan, and A. Kahn, "Direct determination of the hole density of states in undoped and doped amorphous organic films with high lateral resolution," Phys. Rev. Lett. **95**(25), 256405 (2005).

[10] Y. Rosenwaks, R. Shikler, Th. Glatzel, and S. Sadewasser, "Kelvin probe force microscopy of semiconductor surface defects," Phys. Rev. B **70**(8), 085320 (2004).

[11] K. Celebi, P. J. Jadhav, K. M. Milaninia, M. Bora, and M. A. Baldo, "The density of states in thin film copper phthalocyanine measured by Kelvin probe force microscopy," Appl. Phys. Lett. **93**(8), 083308 (2008).

[12] L. Polak and R. J. Wijngaarden, "Two competing interpretations of Kelvin probe force microscopy on semiconductors put to test," Phys. Rev. B **93**(19), 195320 (2016).

[13] U. Celano, Y. Lee, J. Serron, C. Smith, J. Franco, K. Ryu, M. Kim, S. Park, J. Lee, J. Kim, and P. Van Der Heide, "Harnessing charge injection in Kelvin probe force microscopy for the evaluation of oxides," Solid-State Electron. **185**, 108136 (2021).

[14] L. Polak and R. J. Wijngaarden, in *Kelvin Probe Force Microscopy*, edited by S. Sadewasser and T. Glatzel (Springer International Publishing, Cham, 2018), pp. 227–247.

[15] T. Glatzel, U. Gysin, and E. Meyer, "Kelvin probe force microscopy for material characterization," Microscopy **71**(Supplement_1), i165–i173 (2022).

[16] B. H. Lee, K.-S. Cho, D.-Y. Lee, A. Sohn, J. Y. Lee, H. Choo, S. Park, S.-W. Kim, S. Kim, and S. Y. Lee, "Investigation on energy bandgap states of amorphous SiZnSnO thin films," Sci. Rep. **9**(1), 19246 (2019).

[17] X. Shi, C. Lu, G. Xu, G. Yang, N. Lu, Z. Ji, D. Geng, L. Li, and M. Liu, "Thickness of accumulation layer in amorphous indium–gallium–zinc oxide thin-film transistors by Kelvin Probe Force Microscopy," Appl. Phys. Lett. **114**(7), 073501 (2019).

[18] C. Chen and J. Kanicki, "Surface potential study of amorphous In–Ga–Zn–O thin film transistors," J. Appl. Phys. **108**(11), 114508 (2010).

[19] M. Brouillard, N. Bercu, U. Zschieschang, O. Simonetti, R. Mittapalli, H. Klauk, and L. Giraudet, "Experimental determination of the lateral resolution of surface electric potential measurements by Kelvin probe force microscopy using biased electrodes separated by a nanoscale gap and application to thin-film transistors," Nanoscale Adv. **4**(8), 2018–2028 (2022).

[20] W. S. C. Roelofs, S. G. J. Mathijssen, R. A. J. Janssen, D. M. de Leeuw, and M. Kemerink, "Accurate description of charge transport in organic field effect transistors using an experimentally extracted density of states," Phys. Rev. B **85**(8), 085202 (2012).

[21] Y. Zhang, D. Ziegler, and M. Salmeron, "Charge trapping states at the SiO_2–oligothiophene monolayer interface in field effect transistors studied by Kelvin probe force microscopy," ACS Nano **7**(9), 8258–8265 (2013).

[22] I. Lange, J. C. Blakesley, J. Frisch, A. Vollmer, N. Koch, and D. Neher, "Band bending in conjugated polymer layers," Phys. Rev. Lett. **106**(21), 216402 (2011).

[23] W. Chr. Germs, W. H. Adriaans, A. K. Tripathi, W. S. C. Roelofs, B. Cobb, R. A. J. Janssen, G. H. Gelinck, and M. Kemerink, "Charge transport in amorphous InGaZnO thin-film transistors," Phys. Rev. B **86**(15), 155319 (2012).

[24] Y. Zhu, Y. He, S. Jiang, L. Zhu, C. Chen, and Q. Wan, "Indium–gallium–zinc oxide thin-film transistors: Materials, devices, and applications," J. Semicond. **42**(3), 031101 (2021).

[25] J. F. Wager, "Real- and reciprocal-space attributes of band tail states," AIP Adv. **7**(12), 125321 (2017).

[26] E. K.-H. Yu, S. Jun, D. H. Kim, and J. Kanicki, "Density of states of amorphous In-Ga-Zn-O from electrical and optical characterization," J. Appl. Phys. **116**(15), 154505 (2014).

[27] M. Ghittorelli, Z. M. Kovacs-Vajna, and F. Torricelli, "Physical-based analytical model of amorphous InGaZnO TFTs including deep, tail, and free states," IEEE Trans. Electron Devices **64**(11), 4510–4517 (2017).

[28] Y.-S. Lee, E. K.-H. Yu, D.-H. Shim, H.-S. Kong, L. Bie, and J. Kanicki, "Oxygen flow effects on electrical properties, stability, and density of states of amorphous In–Ga–Zn–O thin-film transistors," Jpn. J. Appl. Phys. **53**(12), 121101 (2014).

[29] T. Hiramatsu, M. Nakashima, E. Kikuchi, N. Ishihara, M. Tsubuku, K. Dairiki, and S. Yamazaki, "Correlation between crystallinity and oxygen vacancy formation in In–Ga–Zn oxide," Jpn. J. Appl. Phys. **55**(2), 021203 (2016).

[30] Y. W. Jeon, S. Kim, S. Lee, D. M. Kim, D. H. Kim, J. Park, C. J. Kim, I. Song, Y. Park, U.-I. Chung, J.-H. Lee, B. D. Ahn, S. Y. Park, J.-H. Park, and J. H. Kim, "Subgap density-of-states-based amorphous oxide thin film transistor simulator (DeAOTS)," IEEE Trans. Electron Devices **57**(11), 2988–3000 (2010).

[31] H. Tsuji, M. Nakata, Y. Nakajima, T. Takei, Y. Fujisaki, and T. Yamamoto, "Extraction of trap densities in amorphous In-Ga-Zn-O thin-film transistors by using efficient surface potential calculations," IEEE Electron Device Lett. **36**(10), 1044–1046 (2015).

[32] T. Cramer, A. Sacchetti, M. T. Lobato, P. Barquinha, V. Fischer, M. Benwadih, J. Bablet, E. Fortunato, R. Martins, and B. Fraboni, "Radiation-tolerant flexible large-area electronics based on oxide semiconductors," Adv. Electron. Mater. **2**(7), 1500489 (2016).

19 April 2024 01:59:51

© Author(s) 2023